Chromosome Research (2007) 15:787–797
DOI: 10.1007/s10577-007-1162-x

Inhibition of transcription at radiation-induced nuclear foci of phosphorylated histone H2AX in mammalian cells

Liudmila V. Solovjeva, Maria P. Svetlova, Vadim O. Chagin & Nikolai V. Tomilin*
Institute of Cytology, Russian Academy of Sciences, Tikchoretskii Av. 4, 194064, St. Petersburg, Russia; Fax: +7-812-2970341; E-mail: nvtom@mail.ru
**Correspondence*

Received 2 May 2007. Received in revised form and accepted for publication by Herbert Macgregor 5 June 2007

Key words: chromatin, DNA repair, heterochromatin, histone H2AX, phosphorylation, repressive histone H3 methylations, transcription

Abstract

Double-strand DNA breaks (DSBs) induced by ionizing radiation can be visualized in human cells using antibodies against Ser-139 phosphorylated histone H2AX (γ-H2AX). Large γ-H2AX foci are seen in the nucleus fixed 1 hour after irradiation and their number corresponds to the number of DSBs, allowing analysis of these genome lesions after low doses. We estimated whether transcription is affected in chromatin domains containing γ-H2AX by following *in vivo* incorporation of 5-bromouridine triphosphate (BrUTP) loaded by cell scratching (run-on assay). We found that BrUTP incorporation is strongly suppressed at γ-H2AX foci, suggesting that H2AX phosphorylation inhibits transcription. This is not caused by preferential association of γ-H2AX foci with constitutive or facultative heterochromatin, which was visualized in irradiated cells using antibodies against histone H3 trimethylated at lysine-9 (H3-K9m3) or histone H3 trimethylated at lysine-27 (H3-K27m3). Apparently, formation of γ-H2AX induces changes of chromatin that inhibit assembly of transcription complexes without heterochromatin formation. Inhibition of transcription by phosphorylation of histone H2AX can decrease chromatin movement at DSBs and frequency of misjoining of DNA ends.

Introduction

In mammalian cells, rapid phosphorylation of histone H2AX at C-terminal serines is induced within the first 3 min after treatment of cells with ionizing radiation (IR) and occurs in megabase chromatin domains around double-strand DNA breaks (DSBs) which can be visualized in the nucleus as large (1–2 μm) γ-H2AX foci (Rogakou *et al*. 1998, 1999). A maximal number of these foci is usually observed at 30–60 min after irradiation, but they are detectable for several hours after DNA damage (Rogakou *et al*. 1999, Nazarov *et al*. 2003). The functional significance of H2AX phosphorylation is suppression of misjoining of radiation-induced DNA ends and chromosome aberrations (Franco *et al*. 2006). Phosphorylated H2AX stimulates recruitment to DSBs of cohesin in G_2 cells (Kim *et al*. 2002) which fixes DNA ends and facilitates recombinational repair (reviewed in Lowndes & Toh 2005). However, in G_1 cells DSBs are mostly repaired by nonhomologous end-joining (NHEJ), and cohesin is not accumulated at DSBs in these cells (Kim *et al*. 2002). Misjoining of DNA ends formed at DSBs in G1 cells may be caused by their relative movement in the nucleus, and chromatin movements at DSBs were actually demonstrated by following γ-H2AX tracks after α-particle irradiation (Aten *et al*. 2004). MRE11

repair complex was implicated in adhesion of DNA ends in G_1 cells and suppression of misjoining (Aten *et al*. 2004; Williams & Tainer 2005), but the causes of chromatin movements at DSBs remain unclear. It is possible that chromatin moves because of continued transcription through megabase genome domains containing DSBs. Transcription occurs at all subnuclear compartments (van Driel & Fransz 2004) and can interfere with DSB adhesion and rejoining. DNA unwinding upon transcription can promote double-strand breakage at sites containing covalently bound topoisomerase II (Fortune & Osheroff 2000).

We studied *in vivo* incorporation of 5-bromouridine triphosphate (BrUTP) into RNA of IR-treated human cells and analysed overlap of this RNA with γ-H2AX foci in the nucleus. We found that BrUTP incorporation is suppressed at γ-H2AX foci, suggesting that phosphorylation of H2AX inhibits transcription. To exclude a possibility that γ-H2AX foci are preferentially formed at facultative or constitutive heterochromatin in which transcription is low, we also compared relative distribution of γ-H2AX foci and chromatin domains containing histone H3 trimethylated at lysine-27 (H3-K27m3) or lysine-9 (H3-K9m3).

Materials and methods

Cell cultures, X-irradiation, 5-bromouridine triphosphate (BrUTP) labelling and fixation

MCF-7 cells were obtained from ATCC, and primary culture of human embryonic fibroblasts (HEF) was obtained from the Russian Cell Culture Collection at the Institute of Cytology RAS. Cells were grown in MEM containing 10% FCS.

DSBs were introduced using the RUM-17 X-ray machine run at 200 kV, 13 mA, 0.5 mm Cu filter. The X-ray dose was estimated using chemical dosimetry.

In run-on transcription experiments BrUTP incorporation into HEF nuclei for the detection of RNA synthesis was performed using a scratch labelling method (Schermelleh *et al*. 2001). Cells were grown on 22×22 mm glass coverslips to subconfluency, then treated with X-rays and incubated at 37°C for 1 hour in a CO_2 incubator. Coverslips with cells were then placed into dry tissue culture dishes and 30 μl of complete culture medium containing BrUTP (Sigma) at the final concentration 5 mM was added to each coverslip. With the tip of a hypodermic needle, a

Table 1. Correlation between γ-H2AX (red signal) and Br-UTP (green signal) in human embryonic fibroblasts

Cell number	IR dose (Gy)	Time after irradiation (h)	Correlation coefficient r (red vs green) and probability p of zero hypothesis[a]
1	0.5	1	$r = -0.5184$, $p = 00.0000$
2	0.5	1	$r = -0.3104$, $p = 0.0000$
3	0.5	1	$r = -0.4397$, $p = 00.0000$
4	0.5	1	$r = -0.2258$, $p = 0.0000$
5	0.5	1	$r = -0.4705$, $p = 0.0002$
6	0.5	1	$r = -0.5375$, $p = 0.0038$
7	0.5	1	$r = -0.5693$, $p = 0.0002$
8	0.5	1	$r = -0.5049$, $p = 0.0007$
9	1	1	$r = -0.3536$, $p = 0.0000$
10	1	1	$r = -0.5199$, $p = 00.0000$
11	1	1	$r = -0.1714$, $p = 0.0000006$
12	1	1	$r = -0.1140$, $p = 0.00003$
13	1	1	$r = -0.1033$, $p = 0.0002$
14	1	1	$r = -0.3020$, $p = 0.0000$
15	1	1	$r = -0.3869$, $p = 0.0042$
16	1	1	$r = -0.4445$, $p = 0.0005$
17	0	–	$r = -0.2888$, $p = 0.0000002$
18	0	–	$r = -0.3732$, $p = 0.0046$
19	0	–	$r = -0.3472$, $p = 0.0049$
20	0	–	$r = -0.4828$, $p = 0.0029$
21	0	–	$r = -0.7140$, $p = 0.00000003$
22	0	–	$r = -0.5233$, $p = 0.0051$

[a]Analysed through profiling of γ-H2AX foci using Image J (NIH); correlation coefficient and probability were calculated using Statistica (StatSoft Co).

series of parallel scratches were made about 0.5 mm apart in two directions: from top to bottom and from left to right. After 10 min the prewarmed fresh culture medium was added to the cells (2 ml to each tissue culture dish 35×10 mm). After incubation for 20 min the cells were washed twice with phosphate-buffered saline (PBS) at room temperature (RT), fixed with ice-cold 4% formaldehyde solution in PBS for 10 min and placed in 70% ethanol at 4°C overnight.

In the experiments for studying the localization of γ-H2AX and histone H3 modifications, MCF-7 or HEF cells were incubated in growth medium for 1, 2 or 5 h, washed twice with PBS, treated for 1 min with 0.1% Triton X-100 solution in PBS at room temperature, rinsed with PBS, fixed with 4% formaldehyde solution and placed in 70% ethanol as described above.

Immunofluorescence

After 70%-ethanol storage at 4°C, the coverslips with fixed cells were rinsed with PBS, treated for 15 min with 0.5% Triton X-100 in PBS with shaking at room temperature, then rinsed with PBS. For cells that incorporated BrUTP, diethyl pyrocarbonate-treated PBS was used for all steps of the staining procedure. The coverslips were incubated in 1% Blocking Reagent (Roche, cat. no. 1096 176) in PBS with 0.02% Tween 20 for 30 min at 37°C. Antibodies were diluted with 0.5% Blocking Reagent (Roche) solution with 0.02% Tween 20. The incubations were performed at 37°C, and between subsequent incubations the slides were washed by shaking for 30 min in PBS supplemented with 0.1% Tween 20. The staining of primary HEF for incorporated BrUTP was performed as follows. Cells were incubated with a mixture of monoclonal mouse anti-bromodeoxyuridine antibody (Roche, 1:100) plus custom rabbit polyclonal anti-γ-H2AX antibodies (1:600) for 1 h. After washing, Alexa Fluor 568-conjugated polyclonal goat anti-rabbit IgG (Molecular Probes, 1:400) mixed with biotin-conjugated sheep anti-mouse IgG (Sigma, 1:100) was added for 40 min followed by a final incubation for 40 min with FITC-conjugated avidin (Roche, 1:200). Custom rabbit antibodies

Table 2. Correlation between γ-H2AX (red signal) and H3-K9m3 (green signal) in MCF-7 cells

Cell number	IR dose (Gy)	Time after irradiation (hours)	Correlation coefficient r (red vs. green), and probability p of zero hypothesis[a]
1	1	1	$r = -0.0731$, $p = 0.1308$
2	1	1	$r = 0.0498$, $p = 0.2796$
3	1	1	$r = 0.1244$, $p = 0.0091$
4	1	1	$r = 0.0597$, $p = 0.1878$
5	1	1	$r = -0.3107$, $p = 0.0004$
6	1	1	$r = 0.0650$, $p = 0.2899$
7	1	1	$r = -0.2038$, $p = 0.0050$
8	1	1	$r = 0.0323$, $p = 0.6164$
9	1	2	$r = 0.1663$, $p = 0.00002$
10	1	2	$r = 0.0396$, $p = 0.3499$
11	1	2	$r = -0.0167$, $p = 0.6934$
12	1	2	$r = -0.1807$, $p = 0.000002$
13	1	2	$r = -0.0702$, $p = 0.3836$
14	1	2	$r = 0.0583$, $p = 0.3644$
15	1	2	$r = 0.0363$, $p = 0.5198$
16	1	2	$r = -0.1925$, $p = 0.0980$
17	1	5	$r = -0.0368$, $p = 0.4935$
18	1	5	$r = 0.3304$, $p = 0.000004$
19	1	5	$r = 0.1340$, $p = 0.0066$
20	1	5	$r = 0.0727$, $p = 0.0936$
21	1	5	$r = 0.0704$, $p = 0.2249$
22	1	5	$r = 0.3667$, $p = 0.00002$
23	1	5	$r = -0.1167$, $p = 0.0411$
24	1	5	$r = 0.0993$, $p = 0.1315$

[a]Analysed through profiling of γ-H2AX foci using Image J (NIH); correlation coefficient and probability were calculated using Statistica (StatSoft Co).

against γ-H2AX were described in our earlier paper (Tomilin *et al*. 2001). Slides were mounted in CITIFLUOR antifading solution (glycerol/PBS solution, UKS Chemical Laboratories, UK).

MCF-7 cells were doubly labelled for γ-H2AX and histone H3 trimethylated at lysine-9 (H3-K9m3) in the following way: after fixation the cells were incubated with the mixture of mouse monoclonal anti-phospho-histone H2AX (Ser 139) antibodies (UPSTATE, 1:350) and rabbit polyclonal anti-H3-K9m3 antibodies (Abcam, 1:200) for 1 h. Then cells were incubated with Alexa Fluor 568-conjugated polyclonal goat anti-mouse IgG antibodies (Molecular Probes, 1:400, 40 min) mixed with Cy 2-conjugated goat anti-rabbit IgG antibodies (Jackson ImmunoResearch Laboratories, 1:400). To label H3-K27m3 we used specific rabbit polyclonal antibodies from UPSTATE (1: 100), and the method of double labelling was the same as described above for the double labelling of H3-K9m3 and γ-H2AX.

HEF cells were doubly labelled for γ-H2AX and H3-K27m3 using the same primary antibodies, but the second layer of antibodies was the mixture of Alexa Fluor 568-conjugated polyclonal goat anti-rabbit IgG antibodies (Molecular Probes, 1:400) and Alexa Fluor 488-conjugated polyclonal goat anti-mouse IgG antibodies (Molecular Probes, 1:400, 40 min).

Microscopy

Confocal images of cells were acquired with either a Zeiss confocal laser scanning system LSM 5 Pascal equipped with Axiovert 200M microscope with Plan-NEOFLUAR 100/1.3 objective, or a Leica TCS SL system equipped with DMRE microscope with HCX PL APO 63/1.32 objective. For detection of fluorochromes, a helium-neon laser of 543 nm wavelength and an argon laser of 458/488 nm wavelengths with appropriate filter sets were used. In all cases the optical slice was less than 0.9 μm. Depending on digital zoom, pixel dimensions were 20 or 116 nm (see legends to figures). For the analysis presented in Tables 1, 2, 3 and 4 pixel size was 20, 116, 116, and 58 nm, respectively.

Table 3. Correlation between γ-H2AX (red signal) and H3-K27m3 (green signal) in MCF-7 cells

Cell number	IR dose (Gy)	Time after irradiation (hours)	Correlation coefficient r (red vs. green), and probability p of zero hypothesis[a]
1	1	1	$r = -0.0834$, $p = 0.0396$
2	1	1	$r = 0.0717$, $p = 0.0598$
3	1	1	$r = -0.1301$, $p = 0.0023$
4	1	1	$r = -0.1152$, $p = 0.0153$
5	1	1	$r = 0.0513$, $p = 0.3659$
6	1	1	$r = -0.0700$, $p = 0.2300$
7	1	1	$r = 0.2269$, $p = 0.0010$
8	1	1	$r = -0.0055$, $p = 0.9440$
9	1	2	$r = -0.0161$, $p = 0.7203$
10	1	2	$r = -0.0768$, $p = 0.0734$
11	1	2	$r = -0.0200$, $p = 0.6291$
12	1	2	$r = 0.1458$, $p = 0.0053$
13	1	2	$r = -0.1235$, $p = 0.0996$
14	1	2	$r = 0.0193$, $p = 0.7927$
15	1	2	$r = -0.0001$, $p = 0.9984$
16	1	2	$r = 0.0725$, $p = 0.2326$
17	1	5	$r = -0.1578$, $p = 0.0238$
18	1	5	$r = -0.1100$, $p = 0.0094$
19	1	5	$r = -0.0391$, $p = 0.3435$
20	1	5	$r = 0.0528$, $p = 0.2227$
21	1	5	$r = 0.0969$, $p = 0.1502$
22	1	5	$r = -0.0721$, $p = 0.4244$
23	1	5	$r = -0.0648$, $p = 0.2932$
24	1	5	$r = -0.0184$, $p = 0.7532$

[a]Analysed through profiling of γ-H2AX foci using Image J (NIH); correlation coefficient and probability were calculated using Statistica (StatSoft Co).

Table 4. Correlation between γ-H2AX and H3-K27m3 signals in human embryonic fibroblasts

Cell number	IR dose (Gy)	Time after irradiation (hours)	Correlation coefficient r and probability p of zero hypothesis[a]
1	1	1	$r = -0.0118$, $p = 0.7431$
2	1	1	$r = -0.1295$, $p = 0.0039$
3	1	1	$r = 0.0254$, $p = 0.4930$
4	1	1	$r = -0.0111$, $p = 0.7532$
5	1	1	$r = 0.2017$, $p = 0.0000$
6	1	1	$r = 0.2068$, $p = 0.0000$
7	1	1	$r = 0.0205$, $p = 0.7173$
8	1	1	$r = -0.1289$, $p = 0.0002$
9	1	2	$r = 0.0617$, $p = 0.1757$
10	1	2	$r = 0.0581$, $p = 0.2196$
11	1	2	$r = -0.0531$, $p = 0.1805$
12	1	2	$r = -0.1128$, $p = 0.0041$
13	1	2	$r = 0.1280$, $p = 0.0002$
14	1	2	$r = 0.1318$, $p = 0.0003$
15	1	2	$r = 0.0697$, $p = 0.1084$
16	1	2	$r = 0.0982$, $p = 0.0118$
17	1	5	$r = -0.0684$, $p = 0.1011$
18	1	5	$r = -0.0903$, $p = 0.0204$
19	1	5	$r = 0.1135$, $p = 0.0080$
20	1	5	$r = 0.0470$, $p = 0.3213$
21	1	5	$r = -0.0282$, $p = 0.4288$
22	1	5	$r = -0.0246$, $p = 0.5863$
23	1	5	$r = 0.1173$, $p = 0.0003$
24	1	5	$r = 0.1083$, $p = 0.0015$

[a]Analysed through profiling of γ-H2AX foci using Image J (NIH); correlation coefficient and probability were calculated using Statistica (StatSoft Co).

Results

Analysis of 5-bromouridine triphosphate incorporation at γ-H2AX foci (*run-on transcription assay*)

Transcription *in situ* can be detected by immunofluorescent visualization of 5-bromouridine triphosphate (BrUTP) microinjected into living cells (Verschure *et al*. 1999) or loaded by scratching with a needle (Schermelleh *et al*. 2001). Incorporated BrUTP (nascent RNA) is usually detectable in a large number of sites homogeneously scattered throughout all chromosome territories including gene-dense and gene-poor domains (Sadoni & Zink 2004; van Driel & Fransz 2004). We examined whether the distribution of nascent RNA sites was affected by pretreatment of HEF cells with ionizing radiation (IR) inducing DSBs which were visualized using antibodies against γ-H2AX. In most of γ-H2AX foci that appeared 1 hour after 0.5 Gy (Fig. 1A) or 1.0 Gy (Fig. 1B) of IR, BrUTP incorporation (during the subsequent 20 min) was found to be suppressed. This is apparent from very little yellow overlap between red signal (γ-H2AX foci) and green signal (BrUTP) on confocal images of nuclei (Fig. 1A,B) and is clearly seen on serial confocal sections (Fig. 1C). Control unirradiated cells also showed suppression of BrUTP incorporation at of γ-H2AX foci (Fig. 1D). Fluorescence from adjacent red and green foci was also directly resolved upon microscopy using the Zeiss LSM5 Pascal software (Fig. 2) indicating that little overlap between the two signals is not a consequence of image processing.

To quantitate correlation between γ-H2AX and transcription on images of doubly labelled cells we used ImageJ software obtained from the National Institutes of Health, Bethesda, MD, USA, and STATISTICA (StatSoft Co.). Figure 3 shows an example of quantitation of a profile across the nucleus obtained using ImageJ (Fig. 3A, yellow line) where data from the red and green channels were exported and plotted. We found strong negative correlation between them (Fig. 3B), and similar analysis of many different cells (Table 1) also showed strong negative correlation between γ-H2AX and BrUTP incorporation in IR-treated and unirradiated cells.

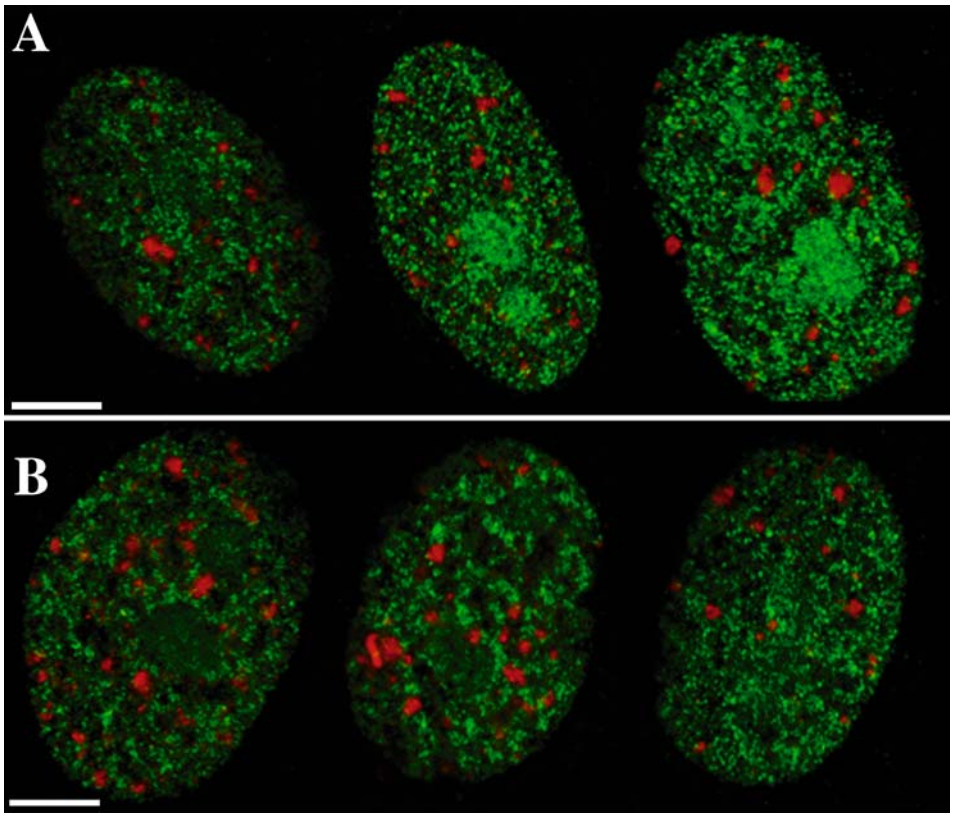

Figure 1. Simultaneous visualization of transcription (green) and phosphorylated histone H2AX (red) in human embryonal fibroblasts treated with 0.5 Gy **A** or 1 Gy **B**, **C** of ionizing radiation. **D** shows unirradiated control cells. Conventional confocal images of different nuclei are shown in **A**, **B** and **D**; **C** shows serial ~0.6 μm confocal sections through one nucleus. Pixel dimensions: $x = y = 20$ nm. Bar = 5 μm.

Little overlap between γ-H2AX foci and H3-K9m3 domains

Low intensity of transcription at radiation-induced γ-H2AX foci may be a consequence of preferential association of these foci with constitutive or facultative heterochromatin which is poorly transcribed. Although radiation-induced DSBs should be randomly distributed in the nuclear space, H2AX phosphorylation may be shifted towards compact chromatin. Constitutive heterochromatin in mammalian cells is hallmarked by trimethylation of histone H3 at lysine-9 (H3-K9m3) (Schotta *et al.* 2004). To analyse possible co-localization of this methylation with γ-H2AX foci we used here double labelling of human MCF-7 cells with antibodies against H3-K9m3 and against phosphorylated H2AX. Since histone H3 methylation can be affected by H2AX phosphorylation, we studied γ-H2AX foci 1 hour as well as 2 and 5 hours after irradiation. It is seen from Fig. 4 that in MCF-7 cells H3-K9m3 (green signal) is associated with large nuclear bodies as well as with small dots distributed throughout the nuclear volume. Large bodies contain high density of DNA, which was detected using parallel staining of MCF-7 cells with DAPI (not shown) and represents compact chromatin (chromocentres). These bodies do not show apparent association with γ-H2AX foci 1 hour after IR (Fig. 4B) and 5 hours after IR (Fig. 4C). Figure 4D shows results of analysis of correlation between the red and green signal in the profile through one nucleus (yellow line in the insert). It is seen (Fig. 4D) that there is no correlation between γ-H2AX and H3-K9m3. Similar analysis of images of other cells (Table 2) showed an absence of correlation or positive as well as negative correlation between the red and green signals in most of analysed nuclei. This indicates that radiation-induced γ-H2AX foci are not preferentially formed in constitutive heterochromatin and may be located elsewhere in the nucleus.

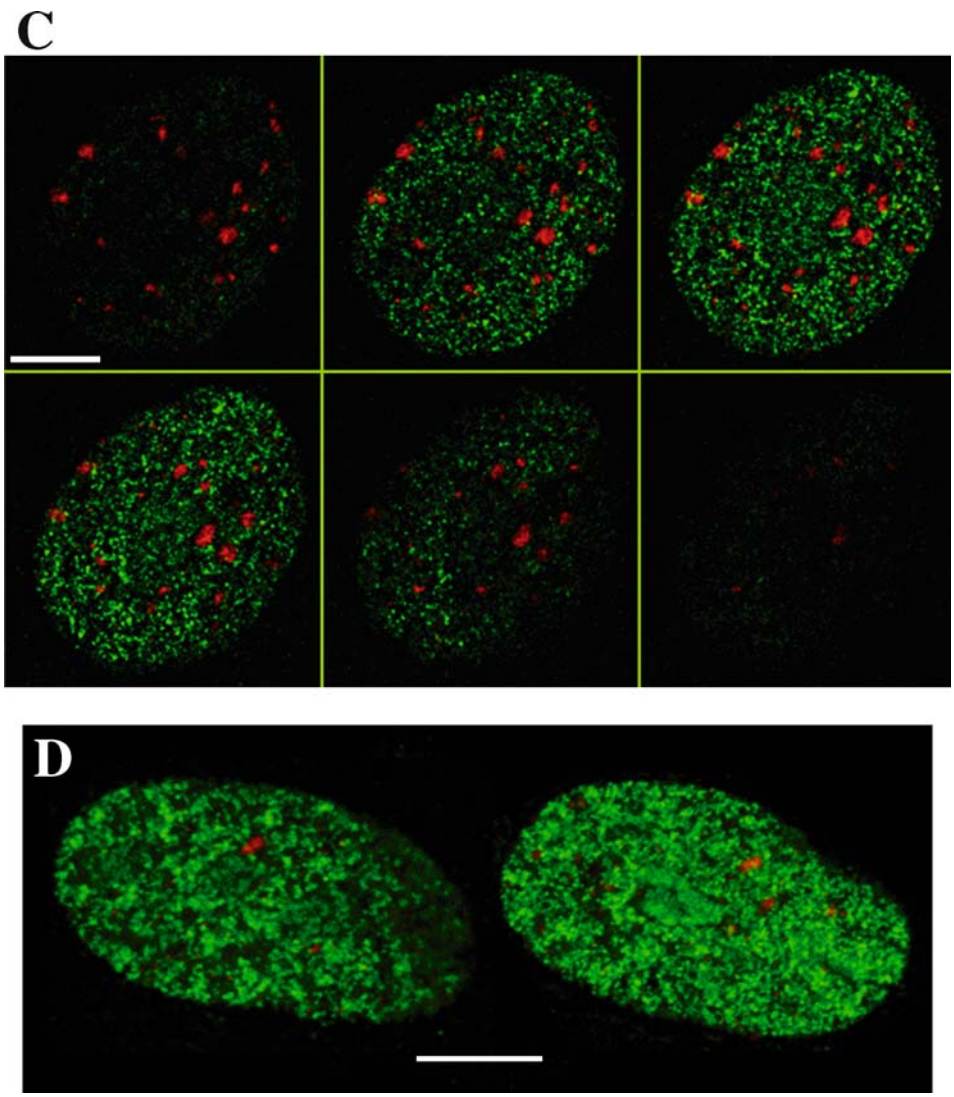

Figure 1. (continued).

No correlation between γ-H2AX foci and facultative heterochromatin

Facultative heterochromatin in mammalian cells is hallmarked by trimethylation of histone H3 at lysine-27 (H3-K27m3) which is present, for example, in the inactive X chromosome in human female cells (Chadwick & Willard 2004).

Figure 5 shows the distribution of H3-K27m3 detected with specific mouse antibodies in MCF-7 (green label) cells as well as γ-H2AX detected with rabbit antibodies (red label). Again, γ-H2AX foci do not show preferential co-localization with H3-K27m3 1 hour (Fig. 5B) or 5 hours (Fig. 5C) after irradiation, which is confirmed by quantitative analysis (Fig. 5D). Profiling of several different cells (Table 3) also showed no correlation of the red and green signals or positive as well as negative correlation between these labels. Similar analysis of correlation between H3-K27m3 and γ-H2AX has been done in experiments with human embryonic fibroblasts and the results (Table 4) also showed no correlation between these labels. It is unlikely, therefore, that the results of experiments with MCF-7 cells (Tables 2 and 3) reflect some special properties of heterochromatin in this cell line. This

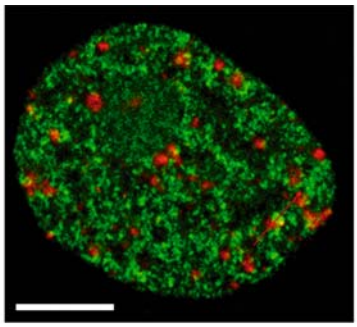

	Marker 1	Marker 2	Difference
Distance	1.77 μm	2.28 μm	0.51 μm
Intensity Ch2-T1	110	190	80
Intensity Ch1-T2	166	65	-101

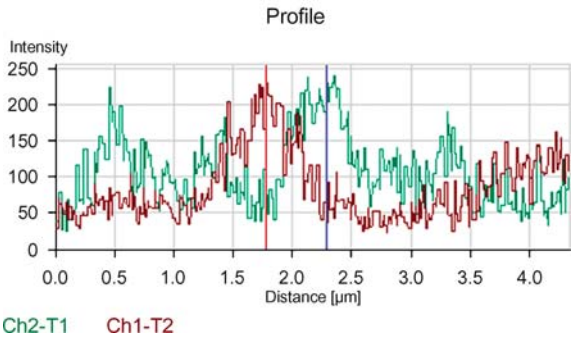

Figure 2. Resolution of green and red fluorescence in the nucleus of an HEF cell double-labelled for transcription (green) and phosphorylated histone H2AX (red) after 1 Gy of ionizing radiation using Zeiss Pascal software. Profile is shown by red line. The table shows intensity and relative position of red and green signals (Ch1-T2 and Ch2-T1, respectively) at vertical red bar (Marker 1) and vertical green bar (Marker 2). Pixel dimensions: $x = y = 20$ nm; optical slice < 0.6 μm. Bar = 5 μm.

indicates that γ-H2AX foci are not preferentially formed in facultative heterochromatin in fibroblasts as well as in MCF-7 cells. It appears, therefore, that negative correlation between γ-H2AX and BrUTP incorporation is caused by H2AX phosphorylation-induced inhibition of transcription and not by preferential localization of γ-H2AX foci in transcriptionally silent chromatin domains.

Discussion

It is shown in this study that incorporation of 5-BrUTP is suppressed at nuclear segments containing radiation-induced γ-H2AX foci. Apparently, some changes of chromatin can lead to inhibition of transcription at γ-H2AX foci, but their nature remains unknown. Changes of chromatin structure and mobility were recently detected at DSB sites in living mammalian cells (Kruhlak *et al*. 2006). Localized adenosine triphosphate-dependent decondensation of chromatin at DSBs established in that study (Kruhlak *et al*. 2006) should, in principle, stimulate local transcription, but in our study we observed inhibition of transcription at DSB sites. Low transcription is typical for compact heterochromatin, but we found that γ-H2AX foci are not preferentially formed in subnuclear domains containing H3-K9m3 or H3-K27m3. It appears, therefore,

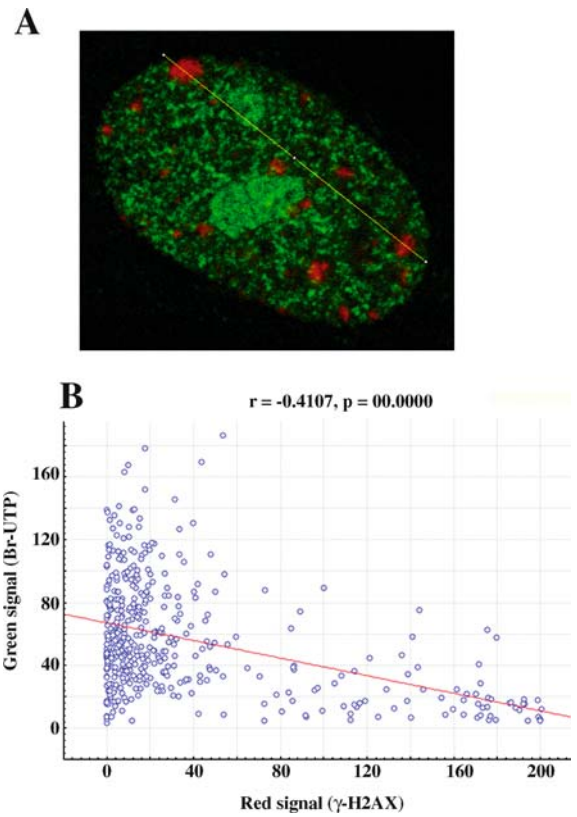

Figure 3. Correlation between transcription (green signal) and histone H2AX phosphorylation (red signal) in a single profile (yellow) through a double labelled nucleus **A** of an HEF cell. Signals were quantitated using the program ImageJ (NIH). The colour RGB image was first transformed into an RGB stack, then the profile through γ-H2AX foci (red) was plotted and the corresponding list of numbers exported. Then the same profile was analysed in the green channel (transcription) and the list of numbers was also exported. Correlation coefficient between these lists of numbers from a single profile through the same cell and probability (r and p) were calculated using the program STATISTICA **B**. Pixel dimensions: $x = y = 20$ nm.

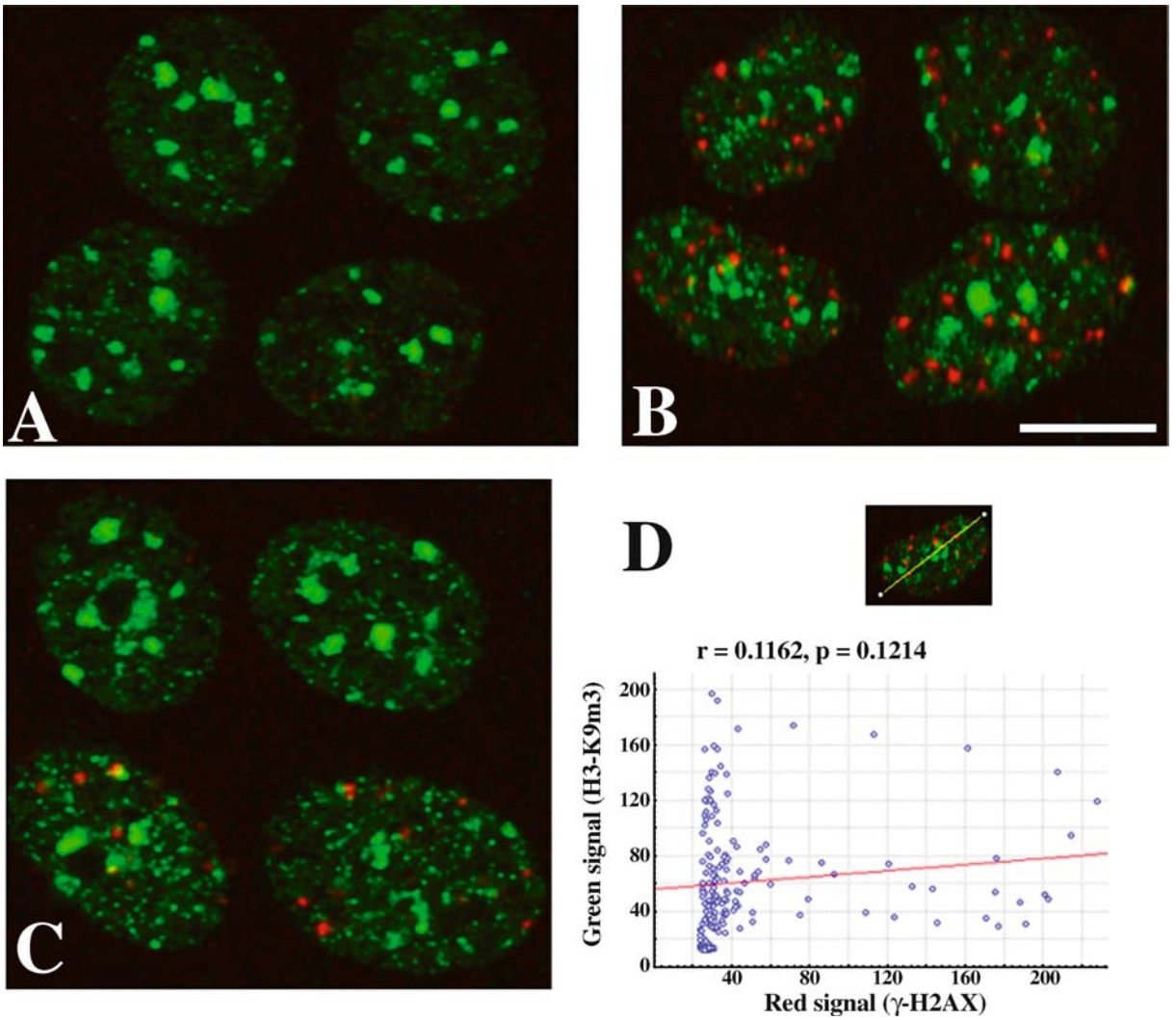

Figure 4. Simultaneous visualization of histone H3 trimethylation at lysine-9 (H3-K9m3, green) and phosphorylated histone H2AX (red) in human MCF-7 cells. **A** shows control unirradiated cells; **B** shows cells 1 hour after 1 Gy of ionising radiation; **C** shows cells 5 hours after 1 Gy of irradiation; **D** shows results of analysis of correlation between green and red signals in a single profile through one nucleus (yellow line in the top insert). Pixel dimensions: $x = y = 116$ nm; optical slice < 0.9 μm. Bar = 5 μm.

that the inhibition of transcription by H2AX phosphorylation is not associated with repressive histone modifications characteristic for constitutive (H3-K9m3) or facultative (H3-K27m3) heterochromatin.

We have shown earlier (Siino *et al*. 2002) that reconstituted chromatin containing human histone H2AX has the same physical properties as H2A-containing chromatin including nucleosome spacing and accessibility to micrococcal nuclease. Other workers recently found that replacement of serine 129 with glutamic acid or deletion of C-end in the yeast histone H2A (homologue of mammalian H2AX) has no effect on nucleosome positioning in minichromosomes and genomic loci, no effect on chromatin stability measured by conventional nuclease digestion, and no effect on DNA accessibility and repair of UV-induced DNA lesions (Fink *et al*. 2007). These data argue against a general role of the C-terminal tails in chromatin organization and suggest that phosphorylated H2A (γ-H2AX) acts by

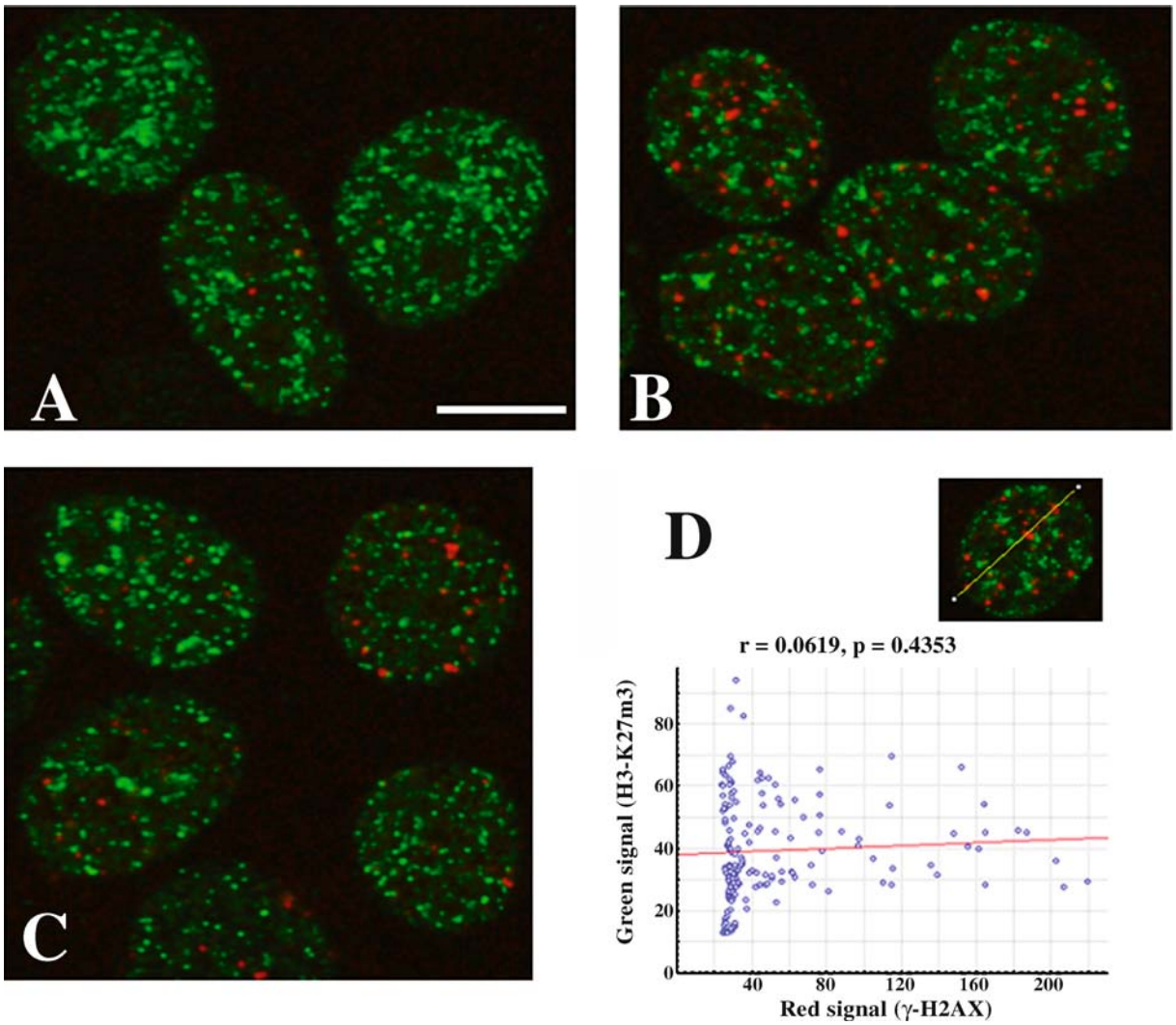

Figure 5. Simultaneous visualization of histone H3 trimethylation at lysine-27 (H3-K27m3, green) and phosphorylated histone H2AX (red) in the human MCF-7 cells. Other designations are the same as described in the legend to Figure 4. Pixel dimensions: $x = y = 116$ nm; optical slice < 0.9 μm. Bar = 5 μm.

changing the efficiency of recruitment of non-histone proteins to chromatin (Fink *et al*. 2007). Initiation of transcription is a stochastic process of low efficiency which is based on transient interactions of transcription factors and RNA polymerases with chromatin (Dundr *et al*. 2002; Kimura *et al*. 2002), and phosphorylation of H2AX can decrease the binding of transcription factors to chromatin near transcription start sites, thus decreasing the efficiency of assembly of transcription complexes on promoters.

It is known that inhibition of transcription in mammalian cells induces DSBs and p53 response (Ljungman *et al*. 1999) as well as phosphorylation of histone H2AX (Casafont *et al*. 2006). In human HeLa cells treated with the inhibitor of transcription actinomycin D, γ-H2AX foci are formed at transcriptionally stalled sites (Mischo *et al*. 2005). It remains unclear whether actinomycin D-induced formation of γ-H2AX foci might be due to the induction of DSB or whether the halt of the elongating polymerase *per se* (followed by its degradation) is sufficient for this effect (Mischo *et al*. 2005). Phosphorylated H2AX present in HeLa cells not treated with actinomycin D can be immunoprecipitated

from nuclear extracts together with RNA polymerase II, suggesting possible functional interactions between these proteins (Mischo *et al*. 2005). However, it is unknown whether radiation-induced γ-H2AX near DSBs can bind RNA polymerase II. This question can be investigated in future studies of links between H2AX phosphorylation and transcription.

Inhibition of transcription by phosphorylation of histone H2AX near DSBs can be important to decrease frequency of misjoining of DNA ends which leads to chromosome aberrations. Chromatin movements can be seen upon analysis of long γ-H2AX tracks in the nuclei treated with ionizing α-particles (Aten *et al*. 2004). If transcription continues at DSBs, it is likely that it will stimulate movements of DNA ends and thus will promote their misjoining. Therefore, inhibition of transcription may facilitate assembly of the flexible scaffold for the repair of DSBs (Williams & Tainer 2005).

Acknowledgements

This research was supported by the Russian Fund of Basic Research grant 07–04–48897, by grant from the FSM programme of the Presidium of the Russian Academy of Sciences, by the Joint Research Center 'Material science and characterization in high technology' and by the INTAS Genomics grant 05–1000004–7753.

References

Aten JA, Stap J, Krawczyk PM *et al*. (2004) Dynamics of DNA double-strand breaks revealed by clustering of damaged chromosome domains. *Science* **303**: 92–95.

Casafont I, Navascues J, Pena E, Lafarga M, Berciano MT (2006) Nuclear organization and dynamics of transcription sites in rat sensory ganglia neurons detected by incorporation of 5′-fluorouridine into nascent RNA. *Neuroscience* **140**: 453–462.

Chadwick BP, Willard HF (2004) Multiple spatially distinct types of facultative heterochromatin on the human inactive X chromosome. *Proc Natl Acad Sci USA* **101**: 17450–17455.

Dundr M, Hoffmann-Rohrer U, Hu Q *et al*. (2002) A kinetic framework for a mammalian RNA polymerase *in vivo*. *Science* **298**: 1623–1626.

Fink M, Imholz D, Thoma F (2007) Contribution of the serine 129 of histone H2A to chromatin structure. *Mol Cell Biol* **27**: 3589–3600.

Fortune JM, Osheroff N (2000) Topoisomerase II as a target for anticancer drugs: when enzymes stop being nice. *Prog Nucleic Acid Res Mol Biol* **6**: 221–253.

Franco S, Gostissa M, Zha S *et al*. (2006) H2AX prevents DNA breaks from progressing to chromosome breaks and translocations. *Mol Cell* **21**: 201–214.

Kim JS, Krasieva TB, LaMorte V, Taylor AM, Yokomori K (2002) Specific recruitment of human cohesin to laser-induced DNA damage. *J Biol Chem* **277**: 45149–45153.

Kimura H, Sugaya K, Cook PR (2002) The transcription cycle of RNA polymerase II in living cells. *J Cell Biol* **159**: 777–782.

Kruhlak MJ, Celeste A, Dellaire G *et al*. (2006) Changes in chromatin structure and mobility in living cells at sites of DNA double-strand breaks. *J Cell Biol* **172**: 823–834.

Ljungman M, Zhang F, Chen F, Rainbow AJ, McKay BC (1999) Inhibition of RNA polymerase II as a trigger for the p53 response. *Oncogene* **18**: 583–592.

Lowndes NF, Toh GW (2005) DNA repair: the importance of phosphorylating histone H2AX. *Curr Biol* **15**: R99–R102.

Mischo HE, Hemmerich P, Grosse F, Zhang S (2005) Actinomycin D induces histone gamma-H2AX foci and complex formation of gamma-H2AX with Ku70 and nuclear DNA helicase II. *J Biol Chem* **280**: 9586–9594.

Nazarov IB, Smirnova AN, Krutilina RI *et al*. (2003) Dephosphorylation of histone gamma-H2AX during repair of DNA double-strand breaks in mammalian cells and its inhibition by calyculin A. *Radiat Res* **160**: 309–317.

Rogakou EP, Pilch DR, Orr AH, Ivanova VS, Bonner WM (1998) DNA double-stranded breaks induce histone H2AX phosphorylation on serine 139. *J Biol Chem* **273**: 5858–5868.

Rogakou EP, Boon C, Redon C, Bonner WM (1999) Megabase chromatin domains involved in DNA double-strand breaks *in vivo*. *J Cell Biol* **146**: 905–916.

Sadoni N, Zink D (2004) Nascent RNA synthesis in the context of chromatin architecture. *Chromosome Res* **12**: 439–451.

Schermelleh L, Solovei I, Zink D, Cremer T (2001) Two-color fluorescence labeling of early and mid-to-late replicating chromatin in living cells. *Chromosome Res* **9**: 77–80.

Schotta G, Lachner M, Sarma K *et al*. (2004). A silencing pathway to induce H3-K9 and H4-K20 trimethylation at constitutive heterochromatin. *Genes Dev* **18**: 1251–1262.

Siino JS, Nazarov IB, Zalenskaya IA, Yau PM, Bradbury EM, Tomilin NV (2002) End-joining of reconstituted histone H2AX-containing chromatin *in vitro* by soluble nuclear proteins from human cells. *FEBS Lett* **527**: 105–108.

Tomilin NV, Solovjeva LV, Svetlova MP *et al*. (2001) Visualization of focal nuclear sites of DNA repair synthesis induced by bleomycin in human cells. *Radiat Res* **156**: 347–354.

van Driel R, Fransz P (2004) Nuclear architecture and genome functioning in plants and animals: what can we learn from both? *Exp Cell Res* **296**: 86–90.

Verschure PJ, van Der Kraan I, Manders EM, van Driel R (1999) Spatial relationship between transcription sites and chromosome territories. *J Cell Biol* **147**: 13–24.

Williams RS, Tainer JA (2005) A nanomachine for making ends meet: MRN is a flexing scaffold for the repair of DNA double-strand breaks. *Mol Cell* **19**: 724–726.